Geoderma 237–238 (2015) 9–20

Contents lists available at ScienceDirect

Geoderma

journal homepage: www.elsevier.com/locate/geoderma

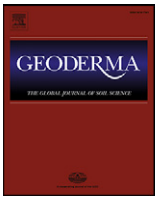

Linking air and water transport in intact soils to macropore characteristics inferred from X-ray computed tomography

Sheela Katuwal [a,*], Trine Norgaard [a], Per Moldrup [b], Mathieu Lamandé [a], Dorthe Wildenschild [c], Lis W. de Jonge [a]

[a] Aarhus University, Department of Agroecology, Blichers Allé 20, DK-8830 Tjele, Denmark
[b] Aalborg University, Department of Civil Engineering, Sohngaardsholmsvej 57, DK-9000, Aalborg, Denmark
[c] Oregon State University, School of Chemical, Biological, and Environmental Engineering, 103 Gleeson Hall, Corvallis, OR 97331-2702, USA

ARTICLE INFO

Article history:
Received 13 March 2013
Received in revised form 9 August 2014
Accepted 15 August 2014
Available online 27 August 2014

Keywords:
Macropores
Limiting-section macroporosity
X-ray computed tomography
Air permeability
5% tracer arrival time

ABSTRACT

Soil macropores largely control fluid and solute transport, making visualization and quantification of macropore characteristics essential for better understanding and predicting soil hydrogeochemical functions. In this study, seventeen large (19 × 20 cm) intact soil cores taken across a loamy field site (Silstrup, Denmark) were scanned at in-situ sampling conditions (~field capacity) at a relatively coarse resolution (500 μm) by medical X-ray computed tomography (CT). In the image analyses, artifacts related to the presence of rocks were identified and removed before linking CT-derived pore parameters to measured fluid transport parameters. After CT scanning, soil cores were saturated and drained at −20 hPa soil–water potential, leaving only pores > 150 μm air-filled. Air permeability (k_{a20}) and air-filled porosity (ε_{20}) were measured to evaluate gas transport behavior in macropore networks under these conditions. Finally, tracer transport experiments at a constant, high flow rate (10 mm h^{-1}) were carried out, and the arrival time for 5% of the applied tracer ($T_{5\%}$) was used as an index for the magnitude of water transport in macropores. Although X-ray CT scanning only identified 5–25% of the total air-filled pore network at −20 hPa, CT-derived macroporosity (average for whole column) and macroporosity for the limiting-quarter section of each column were highly correlated to both k_{a20} and $T_{5\%}$ (R^2 from 0.6 to 0.8). The CT-inferred limiting depth for soil–gas transport was typically located at 90–165 mm depth, and likely a result of soil management history. Results suggest that the functional macropore network for fluid transport was well quantified by rapid, coarse-resolution X-ray CT scanning. Linking rapid X-ray CT scanning with classical fluid transport measurements on large intact columns thus proves highly useful for characterizing soil macropore functions and in perspective may prove to be useful in predicting field-scale variations in gas, water, and chemical transport.

1. Introduction

Macropores – earthworm burrows, root channels, fissures and interaggregate voids – represent only a small fraction of the total porosity in soil, but play a central role in many physical processes like fluid flow and solute transport. Consequently, a good understanding of the determinism of macropores in space and time, and of the physical processes associated with the presence and the geometry of macropores is needed to maintain acceptable crop yield and to prevent environmental pollution. As emphasized by Jarvis (2007) and references therein, rapid flow and solute transport through macropores have been extensively explored by soil scientists during the last few decades. Macropores have been described through functional soil properties such as water retention, air permeability, gas diffusivity, and saturated and unsaturated hydraulic conductivity (Ball, 1981; Blackwell et al., 1990; Granovsky and McCoy, 1997), and by performing tracer experiments in the field or for soil cores in the lab (Deeks et al., 2008; Ersahin et al., 2002; Kjaergaard et al., 2004). In such studies, models for fluid mechanics in porous media helped in assessing the size distribution and the (likely) shape of the macropores. These studies are very useful, however, all these methods to quantify macropores are based on model assumptions (e.g. the capillary model). A number of studies based on image analysis of two-dimensional sections of soil prepared by impregnation techniques have been conducted to describe macropore characteristics (e.g. Droogers et al., 1998; Singh et al., 1991; Velde et al., 1996). Though some macropore properties can be adequately assessed using sections at different depths, many three-dimensional properties cannot be predicted precisely with these two-dimensional sections (Moreau et al., 1999).

Imaging in three-dimensions and making geometrical measurements of macropores have been successfully carried out using imaging techniques like X-ray computed tomography (e.g. Luo et al., 2010a; Munkholm et al., 2012; Perret et al., 1999), a non-invasive and a

---

[*] Corresponding author.
E-mail address: Sheela.Katuwal@agrsci.dk (S. Katuwal).

http://dx.doi.org/10.1016/j.geoderma.2014.08.006
0016-7061/

non-destructive technique which gives information of the spatial variation of the density of a porous medium (Císlerová and Votrubová, 2002). A few recent studies have used X-ray CT to quantify macropore characteristics and link them with soil hydraulic functions (Luo et al., 2008, 2010b; Naveed et al., 2013). In these studies, soil samples from different land uses and management practices or from the same location but with high textural gradients showed considerable variability in gas, water, and solute transport, basically due to large variability of macropore characteristics developed by the management practice or the distinct soil physical properties. Norgaard et al. (2013) and Koestel et al. (2013) studied field-scale variability of soil physical characteristics and solute transport, and found that the strength of preferential flow and enhanced leaching through macropores in the soils was positively correlated with bulk density. The strong preferential transport characteristics in areas with high bulk density were hypothesized to be due to the activation of larger macropores under high irrigation rates used in the study. While the links between soil physical properties (bulk density, soil carbon content and clay content) and preferential transport were well explored in these studies (Koestel et al., 2013; Norgaard et al., 2013), the relations between preferential transport and macropore characteristics were not considered. Imaging of the soil pore space in 3-dimensions and the quantification of pore structure could help in understanding the links between macropore characteristics and fluid flow and solute transport.

In this study, we focus on linking X-ray CT derived pore parameters with fluid transport parameters measured by classical laboratory methods, to facilitate improved understanding of soil macropore networks and their functions. A subset of 17 soil samples from the 65 samples studied by Norgaard et al. (2013) was further investigated for macropore characteristics using a medical CT-scanner. Coarse resolution CT-scanning has suitably been used for investigating macropore features and monitor solute transport in past research (e.g., Perret et al., 1999; Pierret et al., 2002). We hypothesize that coarse resolution scanning can be used in studying possible relations between measured fluid and solute transport characteristics and CT-derived macropore characteristics. In this study, the macropore characteristics derived from a coarse resolution X-ray CT-scanning are combined with measurements of air and solute transport, with the objective of characterizing macropore structure of the intact soil columns, and establishing relationship between macropore characteristics and air and chemical transport parameters.

2. Materials and methods

2.1. Soil samples

Seventeen undisturbed soil samples (19 cm diameter and 20 cm in height) from the top soil of an agricultural field, 185 m long and 91 m wide in Silstrup (56° 55′56″ N, 8° 38′44″ E), Denmark were used in the study. The agricultural field had a natural gradient in total organic carbon content (0.017–0.022 kg kg^{-1}), clay content (0.14–0.19 kg kg^{-1}), and bulk density (1.39–1.60 g cm^{-3}) along the length of the field (Norgaard et al., 2013). The 17 soil cores studied (25% of those studied by Norgaard et al. (2013) for the mapping of soil physical–chemical and structural parameters) were chosen so as to obtain samples with a variability in organic carbon, clay content, and bulk density, representing the variability found in the field. For this selection, we used the “subset features” function of the Geostatistical Analyst Tool in ArcGis 10.1 (Esri, Redlands, CA, USA). Undisturbed soil cores were sampled by driving aluminum rings vertically into the soil with the hydraulic press of a tractor until the top of the ring was level with the soil surface. The samples were manually excavated, trimmed at the bottom, sealed with plastic caps at both ends and stored at 2 °C prior to analysis. The site was not cleared off of any vegetation before sampling, thus the structure of the topsoil was preserved in the soil samples. The soil cores consisted of sandy loam and loam soil (USDA soil textural classification system). The field was under red fescue (*Festuca rubra* L.) with no soil management for about 2 years prior to sampling. The soil was close to field capacity with moisture content ranging from 0.32 to 0.35 cm^3 cm^{-3} at the time of sampling. The physical properties of the soil samples are presented in Table 1.

2.2. Air permeability

Intrinsic air permeability, hereafter referred to as air permeability (k_a), was determined with an air permeameter by measuring the air flow rate through the sample under a constant pressure head difference of 5 cm across the sample length as described by Iversen et al. (2001). The air permeability was calculated using Darcy's law as:

$$Q = A\frac{k_a}{\eta}\frac{\Delta P}{L} \tag{1}$$

where Q is the air flow rate [L^3 T^{-1}], A is the cross-sectional area of the soil [L^2], k_a is the air permeability [L^2], η is the dynamic air viscosity [M L^{-1} T^{-1}] corrected for temperature, ΔP is the pressure difference [M L^{-1} T^{-2}], and L is the sample length [L]. The air permeability was measured at a water matric potential of −20 hPa relative to the mid-section of the 20-cm high column and is denoted as k_{a20}. To obtain the matric potential of −20 hPa, the samples were placed in a sandbox with an artificial soil–water solution (0.652 mM NaCl, 0.025 mM KCl, 1.842 mM $CaCl_2$ and 0.255 mM $MgCl_2$; pH = 6.38; EC = 0.6 mmho) and slowly saturated from the bottom for 3 days. The samples were then drained to −20 hPa matric potential relative to the mid-section of the column for 3 days. At this matric potential, the soil water tension along the column height would vary between −10 hPa and −30 hPa.

2.3. Leaching experiment

The leaching experiments were carried out after the samples were drained to −20 hPa matric potential relative to the mid-section of the column. Artificial rainwater (0.012 mM $CaCl_2$, 0.015 mM $MgCl_2$ and 0.121 mm NaCl; EC = 22.5–27 μmho; pH = 5.76–7.26) was applied to the top of the soil column with a rotating irrigation head which was equipped with 44 needles placed randomly. Irrigation was applied for 6.5 h at an intensity of 10 mm h^{-1}. The soil column rested on a 1-mm stainless steel screen and thus was subjected to free drainage. The effluent was collected in plastic bottles placed underneath the soil columns

Table 1
General physical properties of the soil samples.

Column no.	Clay (<2 μm) (kg kg^{-1})	Silt (2–50 μm) (kg kg^{-1})	Organic carbon (kg kg^{-1})	Bulk density (mg m^3)	Porosity (cm^3 cm^{-3})
1	0.153	0.315	0.021	1.57	0.41
2	0.154	0.307	0.020	1.53	0.42
3	0.147	0.314	0.021	1.48	0.44
8	0.148	0.322	0.020	1.39	0.48
19	0.148	0.332	0.019	1.48	0.44
20	0.148	0.302	0.019	1.42	0.46
26	0.149	0.307	0.021	1.42	0.46
31	0.175	0.302	0.022	1.45	0.45
32	0.175	0.327	0.022	1.44	0.46
44	0.176	0.299	0.020	1.43	0.46
47	0.174	0.298	0.018	1.59	0.4
48	0.176	0.33	0.021	1.47	0.45
54	0.168	0.288	0.019	1.47	0.45
55	0.174	0.303	0.018	1.6	0.4
59	0.172	0.268	0.020	1.52	0.43
73	0.162	0.29	0.021	1.42	0.47
75	0.182	0.325	0.019	1.47	0.45
Mean	0.164	0.308	0.020	1.48	0.44
(σ)	(0.013)	(0.017)	(0.001)	(0.06)	(0.02)